Journal of Biomechanics 118 (2021) 110295

Contents lists available at ScienceDirect

Journal of Biomechanics

journal homepage: www.elsevier.com/locate/jbiomech
www.JBiomech.com

A computational study of fatigue resistance of nitinol stents subjected to walk-induced femoropopliteal artery motion

R. He [a], L.G. Zhao [a,*], V.V. Silberschmidt [a], H. Willcock [b]

[a] Wolfson School of Mechanical, Electrical and Manufacturing Engineering, Loughborough University, Epinal Way, Loughborough LE11 3TU, UK
[b] Department of Materials, Loughborough University, Epinal Way, Loughborough LE11 3TU, UK

ARTICLE INFO

Article history:
Accepted 23 January 2021

Keywords:
Nitinol stent
Fatigue resistance
Femoropopliteal artery
Finite element
Peripheral artery disease

ABSTRACT

Fatigue resistance of nitinol stents implanted in femoropopliteal arteries is a critical issue because of their harsh biomechanical environment. Limb flexions due to daily walk expose the femoropopliteal arteries and, subsequently, the implanted stents to large cyclic deformations, which may lead to fatigue failure of the smart self-expandable stents. For the first time, this paper utilised the up-to-date measurements of walk-induced motion of a human femoropopliteal artery to investigate the fatigue behaviour of nitinol stent after implantation. The study was carried out by modelling the processes of angioplasty, stent crimping, self-expansion and deformation under diastolic-systolic blood pressure, repetitive bending, torsion and axial compression as well as their combination. The highest risk of fatigue failure of the nitinol stent occurs under a combined loading condition, with the bending contributing the most, followed by compression and torsion. The pulsatile blood pressure alone hardly causes any fatigue failure of the stent. The work is significant for understanding and improving the fatigue performance of nitinol stents through innovative design and procedural optimisation.

© 2021 The Author(s). Published by Elsevier Ltd. This is an open access article under the CC BY license (http://creativecommons.org/licenses/by/4.0/).

1. Introduction

Peripheral artery disease (PAD), narrowing of the peripheral arteries, is caused by the build-up of plaque on the inner wall of a blood vessel, which restricts the blood flow through the lower limbs. PAD is most commonly found in the leg arteries, i.e., femoropopliteal arteries. Angioplasty and stenting are currently recommended for PAD treatment. Angioplasty alone was unsuccessful in about 50% of cases because of the acute elastic recoil, residual stenosis and long-term restenosis (Jeans et al., 1990; Saxon et al., 2003). Balloon-expandable stents reduced failure rates immediately after the deployment by preventing elastic recoil and scaffolding dissection. However, they do not perform well under large biomechanical deformations in the femoropopliteal arteries due to their limited flexibility and susceptibility to permanent deformation under external forces (Heuser and Henry, 2008). The long-term outcomes of stent deployment are also disappointing due to the development of restenosis over time (Henry et al., 1995). As a result, self-expandable nitinol stents were developed, which have excellent flexibility and can recover from deformation thanks to their unique superelastic behaviour. Superelastic nitinol stents provide favourable safety and durability (Vogel et al., 2003; Mewissen, 2004; Duda et al., 2006), and demonstrate superior clinical outcomes when compared to conventional balloon angioplasty (Schillinger et al., 2006; Laird et al., 2010; Fusaro et al., 2013). However, fracture of nitinol stents was frequently observed during follow-up examinations (dos Reis et al., 2019; Kim et al., 2020), which is directly associated with the repetitive external forces, i.e., fatigue loading, exerted on the stents during normal walk (MacTaggart et al., 2014). Generally, loading conditions of stents are very complex and include pulsatile blood pressure, bending, torsion and axial compression that contribute significantly to the high rate of treatment failure (MacTaggart et al., 2014).

Some computational studies have previously been carried out to investigate the fatigue behaviour of nitinol stents. For instance, Harvey (2011) constructed a finite-element (FE) model of an artery, generated from CT angiography to assess the fatigue performance of a stent under pulsatile and articulation loads. The results proved the feasibility of advanced nonlinear FE simulations in fatigue prediction for nitinol stent in human arteries. A research team at Politecnico di Milano (Italy) performed a series of numerical studies on the risk of stent's fatigue failure, focusing on the effects of failure criteria, loading conditions and plaque morphology (Petrini et al., 2012; Meoli et al., 2013; Meoli et al., 2014; Dordoni et al., 2014, 2015; Petrini et al., 2016; Allegretti et al.,

* Corresponding author.
E-mail address: L.Zhao@lboro.ac.uk (L.G. Zhao).

https://doi.org/10.1016/j.jbiomech.2021.110295
0021-9290/© 2021 The Author(s). Published by Elsevier Ltd.
This is an open access article under the CC BY license (http://creativecommons.org/licenses/by/4.0/).

2018). However, in their simulations, an artery and plaque were either excluded or assumed to be isotropic elastic/hyperelastic. Recently, Lei et al. (2019) showed the necessity and feasibility of considering both atherosclerotic plaque and physiological loading conditions in the evaluation of fatigue behaviours of stents, using the FE method. However, their model consisted of only a single-layer arterial wall, assumed to be both isotropic and hyperelastic.

To study the fatigue behaviour of implanted nitinol stents properly, it is essential to understand the biomechanical environment of femoropopliteal artery. Ansari et al. (2013) reviewed some studies regarding the measurements of deformation of human femoropopliteal arteries, and torsion was regarded as the most challenging to measure due to a lack of identifiable arterial markers that can be tracked with limb flexion. Cheng et al. (2006, 2010) and Klein et al. (2009) used a side branch technique to quantify bending, torsion and axial compression of femoropopliteal artery, but their method might significantly underestimate local deformations in places where no branches could be identified. To resolve this problem, MacTaggart et al. (2014), Desyatova et al. (2017) and Poulson et al. (2018) deployed intra-arterial markers in femoropopliteal arteries of cadavers to achieve a higher accuracy of measurements on bending, torsion and axial compression of femoropopliteal artery for walking, sitting and gardening postures. Very recently, the same technique was used to assess the effect of stenting on arterial deformations by calculating differences in foreshortening, bending and twisting between unstented and stented femoropopliteal arteries (MacTaggart et al., 2019). To the authors' best knowledge, these measurements were not used to study fatigue resistance of nitinol stents implanted in femoropopliteal arteries, especially under walking conditions, which is an essential activity for patients.

In this paper, advanced FE simulations were carried out to investigate the fatigue resistance of nitinol stents subjected to walk-induced motion of an femoropopliteal artery. The developed FE models simulated a diseased artery with a layered structure and a self-expandable nitinol stent, all described with advanced constitutive relationships. The study was implemented by modelling the processes of angioplasty, stent crimping, self-expansion and deformation under diastolic-systolic blood pressure, repetitive bending, torsion and axial compression as well as their combination. The cyclic strain in the nitinol stent was fully assessed and used to evaluate the fatigue behaviour.

2. Methodology

2.1. Finite-element model

In our numerical studies, a two-layer femoropopliteal artery, with an overall wall thickness of 1.15 mm, an inner diameter of 4 mm and a length of 50 mm, was modelled. Specifically, the artery consisted of an adventitia and a media layers, with thicknesses of 0.41 mm and 0.74 mm, respectively (Wong et al., 1993). An extremely thin intima layer was not considered in the simulations due to its negligible contributions to artery deformation (He et al., 2020a). The plaque was modelled as a symmetric layer inside the artery, with a length of 18 mm and a stenosis of 50% (i.e., an inner diameter of 2 mm). Hexahedral elements with reduced integration (C3D8R) of Abaqus software were used to mesh the artery and the plaque (Fig. 1a). In the radial direction, the adventitia and media layers, and plaque were meshed with 2, 4 and 8 rows of elements, respectively. In the longitudinal direction, a bias control was used to mesh the artery, allowing for a gradual increase of the element

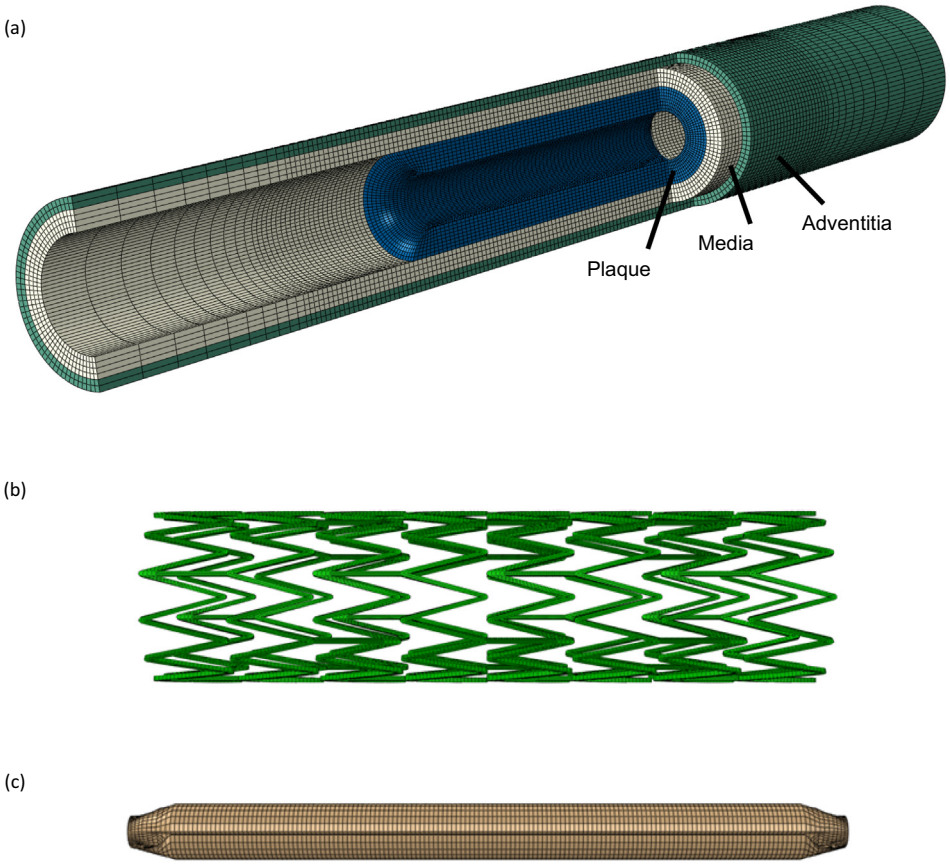


Fig. 1. Finite-element models: (a) femoral artery-plaque assembly; (b) Zilver stent; (c) angioplasty balloon.

size towards both ends of the artery. FE model for the Zilver Flex® Vascular Self-Expanding Stent (Cook Medical, USA) was built using Abaqus CAE, with a length of 20 mm, an outer diameter of 5 mm and a strut thickness of 125 μm (Fig. 1b). The stent was also meshed with C3D8R elements. A linear-elastic tube was created in the numerical model to crimp and release the Zilver stent in the diseased artery.

Clinically, blocked arteries undergo balloon angioplasty before stenting. To simulate angioplasty, a three-folded non-compliant balloon model was also created (He et al., 2020b), with a length of 21 mm and a nominal diameter of 4 mm (Fig. 1c). Three-dimensional 4-node membrane elements with reduced integration (M3D4R) were used to mesh the balloon. We have compared the simulation results with and without angioplasty, and the maximum stress/strain values appear to be lower for the stent when deployed after angioplasty (10% difference). This is because angioplasty introduces pre-dilation to the diseased artery which facilitates the expansion of stent and thus lowers the stress/strain levels in the stent after deployment (see Supplementary Materials). Therefore, angioplasty was considered in our simulations in order to provide a more accurate assessment of the fatigue resistance for nitinol stents.

2.2. Constitutive models

As presented in He et al. (2020b), the modified HGO-C model with damage (Nolan et al., 2014; Fereidoonnezhad et al., 2016) was used to capture the anisotropic hyperelastic behaviour of the arterial layers, especially the stress-softening effect due to tissue damage caused by stenting. The mechanical behaviour of the plaque was introduced in terms of the first-order Ogden model with Mullins effect (Ogden, 1972; Ogden and Roxburgh, 1999). The model parameters for the artery and plaque are given in the Supplementary Materials. The Zilver stent was made of superelastic nitinol (nickel titanium), whose constitutive behaviour was described in Azaouzi et al. (2013). The angioplasty balloon was assumed to be made of polyethylene terephthalate, with a density of 1.4E−9 t/mm^3, Young's modulus of 2000 MPa, and Poisson's ratio of 0.44 (Goodfellow, 2018).

2.3. Boundary conditions

All simulations were implemented with the Abaqus explicit solver (Abaqus, 2017); each employed 160 cores on a high-performance computer cluster and took about one month to finish. Mass scaling was not applied (significant oscillations would occur in stress if mass scaling was used, giving totally unrealistic results), but a default damping coefficient of 1.2 for quadratic bulk viscosity was applied in our simulations to mitigate high-frequency oscillations. Angioplasty was simulated before stenting, with a peak inflating pressure of 1.8 MPa applied to the inner surface of the balloon. Interaction between the balloon and the artery was modelled as a general hard contact with a frictional coefficient of 0.2 (Dordoni et al., 2014). The hard contact in Abaqus ensures no penetration for surfaces in contact; also, there is no restriction to the magnitude of contact pressure that can be transmitted when the surfaces are in contact, as expected for stent deployment. The process of stent deployment in the diseased artery consisted of crimping and releasing steps. The crimping step was performed by applying an inward radial displacement on the tube around the stent to gradually shrink it to an outer diameter of 2 mm. Interaction between the stent and the tube was modelled using the same properties as those used for balloon-artery interaction. Subsequently, the next step was modelled by applying a longitudinal displacement to the tube to gradually remove the tube, thus releasing the stent. Interaction of the stent with the artery was added in this step using the same properties as those used for balloon-artery interaction. Both ends of the artery were fixed in this step to prevent the rigid-body motion.

2.4. Loading conditions

Following the stent deployment, its in-service fatigue behaviour was studied under blood pressure, bending, torsion, axial compression and their combination. Each simulation ran for 3 cycles, except for the blood pressure (20 cycles). In this step, the tube was removed while contact between the stent and artery remained. Blood pressure of 0.01 MPa (diastolic value) was first applied to the inner surfaces of both stent and artery, followed by diastolic-systolic cyclic loading. In this study, the diastolic-systolic blood pressure was modelled in a realistic waveform with fluctuations between a diastolic value of 80 mmHg (0.01 MPa) and a systolic value of 120 mmHg (0.015 MPa; Qiu et al., 2018).

Previously, stenting of the popliteal artery was generally considered inappropriate due to the high mechanical stress and bending of the artery during knee flexion. However, the clinical practice noticed its feasibility and started to perform it in popliteal artery recently (Fargion et al., 2017; San Norberto et al., 2017; Sibé et al., 2017; Elens et al., 2019). Moreover, in this study, the most severe deformations in the femoropopliteal artery (popliteal artery) were taken as the worst case of walking-induced motion with the highest impact on fatigue failure of implanted stents (Desyatova et al., 2017; Poulson et al., 2018; MacTaggart et al., 2019; Fig. 2). The peak loadings of bending, torsion and axial compression were measured by comparing marker positions for the walking (110°) posture to the standing (180°) posture. Markers were deployed approximately 2 cm apart within the *in situ* iliac, femoral and popliteal arteries. We took the mean values of torsion in Desyatova et al. (2017), and axial compression and bending in Poulson et al. (2018) in popliteal artery in walking posture, plus the effects of deployment of Zilver stent in MacTaggart et al. (2019). The loadings for bending, torsion and axial compression are shown in Fig. 3, where the blue and red colours denote the initial and deformed (peak load) conditions, respectively. The two reference points, RP1 and RP2, were used as control points to constrain all the degrees of freedom (except the radial displacement considering the radial deformation of the artery model) of the nodes in the non-stented regions (yellow in Fig. 3), with kinematic coupling. Thus, the stent was not subjected to any boundary effect. Specifically, rotations of ∓39.8° and ∓11.2° around the T- and Z-axis were applied to RP1 and RP2 simultaneously to simulate bending and torsion loadings, respectively. For the axial compression, displacements of ±0.78 mm along the Z-axis was applied to RP1 and RP2 simultaneously. All cyclic loadings had a sine waveform (based on observation of human walking motion; Aoi et al., 2019) with a frequency of 1 Hz (Ji and Pachi, 2005). Constraints of artery ends were removed for these simulations.

In the crimping, releasing and cyclic loading steps, the kinetic energy remained in orders of magnitude of 10^{-6} mJ, 10^{-3} mJ and 10^{-6}–10^{-4} mJ, respectively. Hence, the quasi-static response in the crimping step was ensured, while dynamic response was expected for the releasing and cyclic loading steps.

2.5. Fatigue assessment

The equivalent strain (considering the multiaxial strain state for the stent in our study) was extracted from our FE results and plotted in a constant-life diagram in terms of strain amplitude versus mean strain for each case. The fatigue limit curve was provided in Pelton (2011) and represents a fatigue life of 10^7 cycles, where the slight increase of fatigue life with increasing mean strain (also with some fluctuations at the beginning) for mean strain below 7%

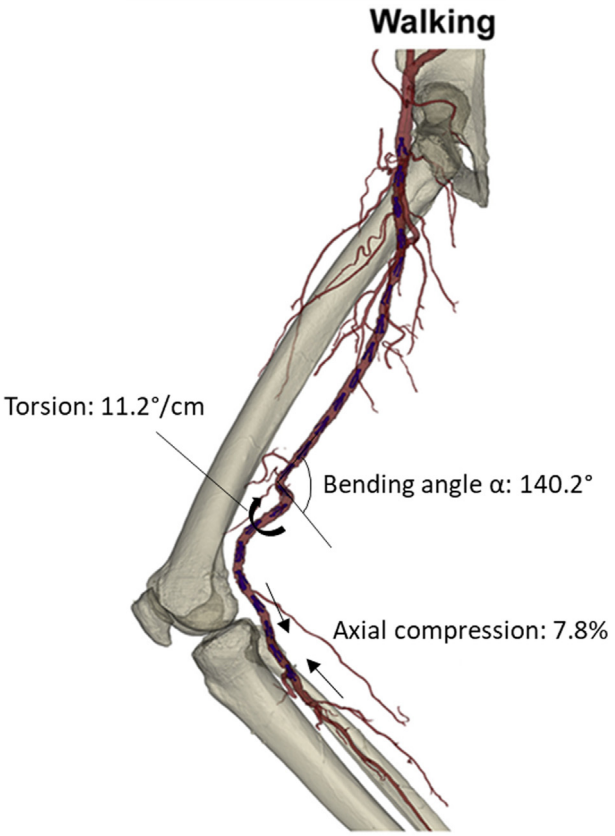


Fig. 2. Computed tomography of the limb flexion states demonstrating walking (110°) posture (Poulson et al., 2018), with most severe deformation in stented femoropopliteal artery during walking (not drawn to the exact positions).

is due to the formation of stress-induced martensite, according to Pelton et al. (2008).

3. Results

3.1. Fatigue performance under blood pressure

The distributions of effective strain in the stent at the end of systole and diastole pressures are plotted in Fig. 4a. The maximum strain in the stent for a systole was higher than that for a diastole (2.23% *vs.* 2.22%). Also, high-level strains (red zones) were mainly found at the inner corner of U-bends in the stent, while low strains (blue zones) occurred in the middle of bridging struts. The results suggested that the inner corners of U-bends had a higher risk of fatigue failure due to blood pressure. The evolution of effective strain at the high-strain region (Fig. 4a) under cyclic systolic-diastolic loading showed that the strain fluctuation tended to stabilize at Cycle 18 (Fig. 4b), with a peak and valley strain of 2.23% and 2.22%, respectively. The stabilised strain condition for all the elements were extracted and plotted in the constant-life diagram (Fig. 4c). Its black line illustrates the fatigue strain limit of nitinol according to Pelton (2011), with the black markers representing the levels of strain amplitude and mean strain of the elements. Apparently, all the elements are in the safe zone, experiencing relatively low levels of strain amplitude and mean strain caused by the pulsatile blood pressure.

3.2. Fatigue performance under bending

In contrast, bending fatigue is a more challenging condition for stents (Fig. 5a) with higher values of the maximum strain corresponding to both the peak load (3.73%) and the unloaded condition (2.35%). Similar to the blood-pressure loading, high (red zones) and

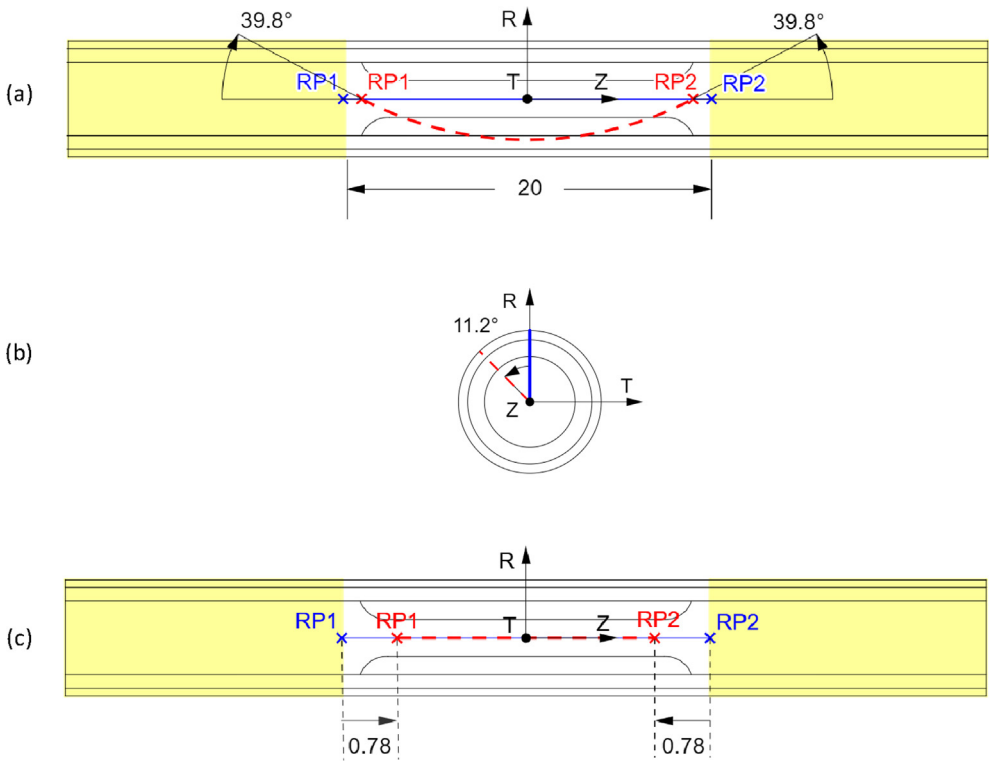


Fig. 3. Schematics of (a) bending, (b) torsion and (c) axial compression (constrained regions: yellow; initial condition: blue; deformed condition: red). All dimensions of length in mm (not to scale).

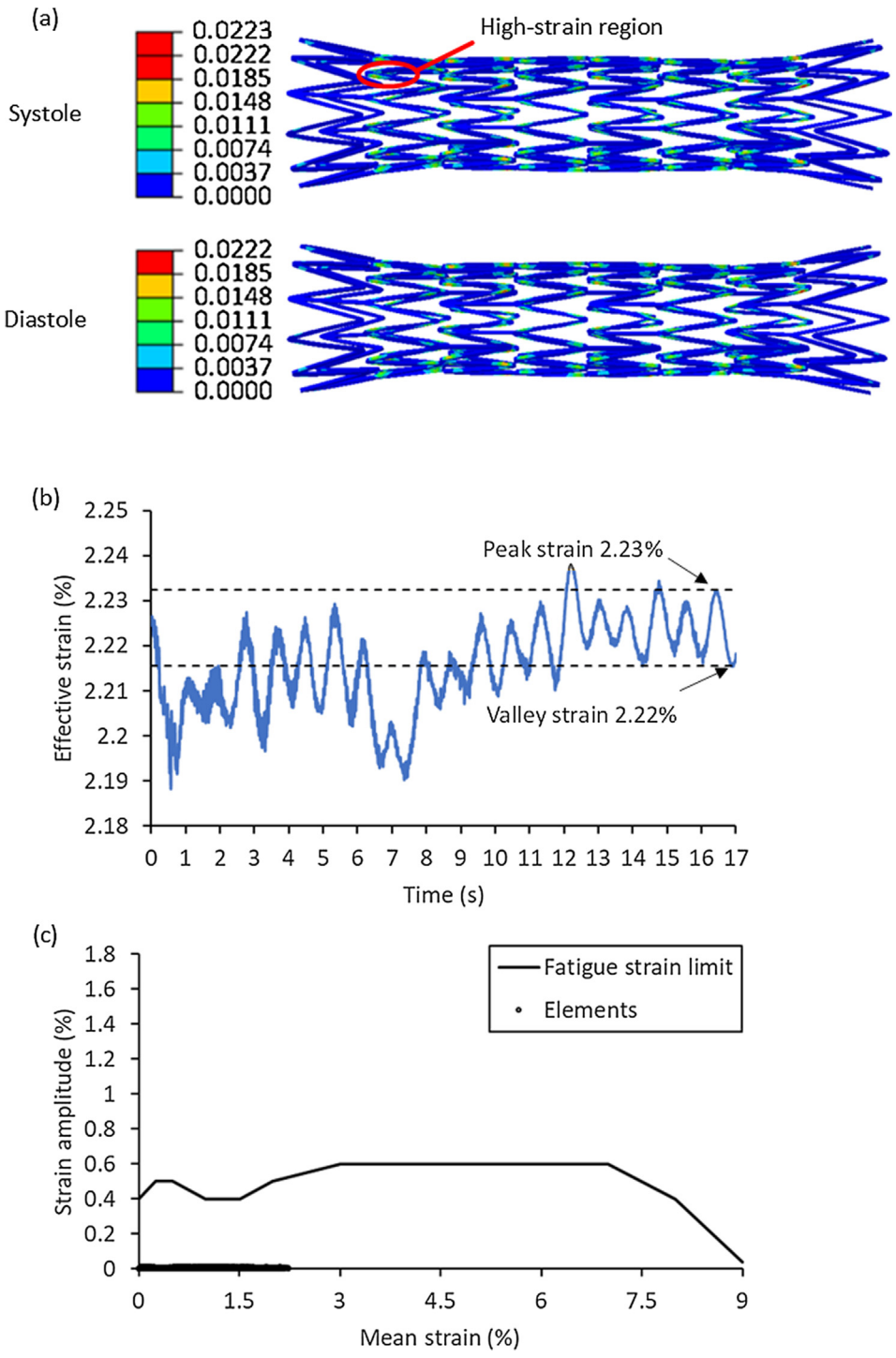


Fig.4. Fatigue performance under blood pressure: (a) contour plots of effective strain in stent at the end of systole and diastole; (b) evolution of effective strain in high-strain region in (a) during systolic-diastolic loading process (time refers to the period of cyclic loading); (c) constant-life diagram.

low (blue zones) strains were found at the inner corner of U-bends and the middle of bridge struts, respectively. The stabilized (after 1 cycle) peak and valley strains for the high strain region (Fig. 5a) were 3.73% and 2.35%, respectively (Fig. 5b). The constant-life diagram (Fig. 5c) demonstrates that, most elements were still in the safe zone, but with much higher mean strain and strain amplitude compared to the results for pulsatile blood pressure. Some elements were even located in the dangerous zone based on the estimated fatigue strain limit line, indicating an increased risk of fatigue failure.

3.3. Fatigue performance under torsion

Fig. 6a shows the effective strain distribution on the stent at peak loading and unloaded conditions under torsion fatigue. The maximum strain in the stent varied between 2.26% (peak load) and 2.24% (unloaded). The distributions of high and low strains (red and blue zones, respectively) were similar to those under the cyclic bending case. Fig. 6b shows the evolution of effective strain at the high strain region (Fig. 6a), which tended to stabilize after 1 cycle. It had lower peak strain (2.26%) and thus smaller

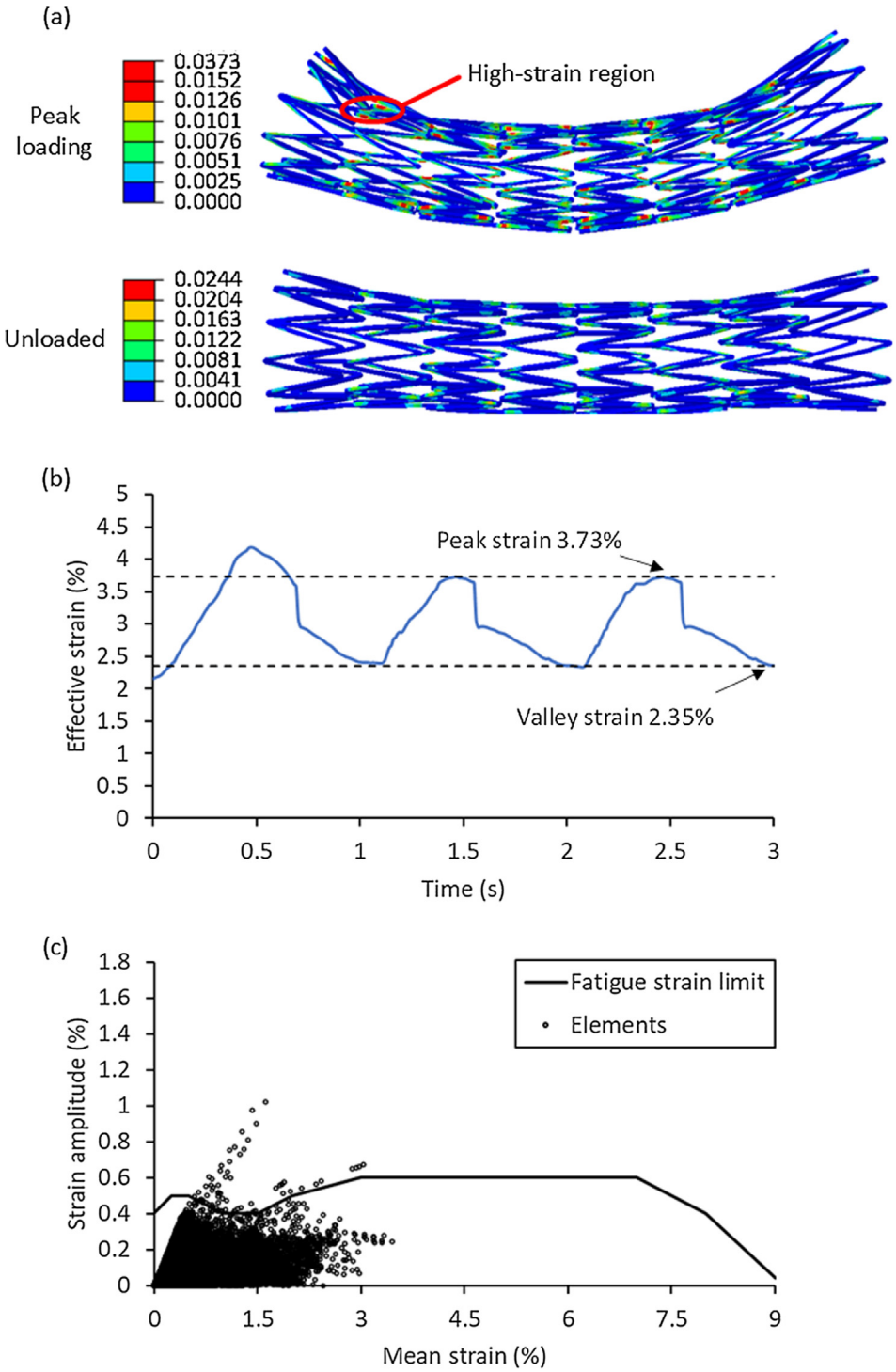


Fig. 5. Fatigue performance under bending: (a) contour plots of effective strain in stent at peak loading and unloaded conditions; (b) evolution of effective strain in high-strain region in (a) where time refers to the period of cyclic loading; (c) constant-life diagram.

strain amplitude (0.13%) than those for the bending case (3.73% and 0.69%), demonstrating a decreased risk of fatigue failure. Such tendency is also reflected in the constant-life diagram (Fig. 6c), where elements are well within the safe zone.

3.4. Fatigue performance under axial compression

Fig. 7a shows the effective strain distribution of the stent at the peak loading and unloaded conditions under axial compression fatigue. Similar to the bending and torsion fatigue, the maximum strain in the stent at the peak load was higher than that at the unloaded condition (3.13% *vs.* 2.52%). The evolution of effective strain at the high strain region (Fig. 7a) subjected to axial compression fatigue is plotted in Fig. 7b, which tended to stabilize after 1 cycle. Its stabilized peak strain and strain amplitude (3.13% and 0.31%) were higher than those for the torsion case (2.26% and 0.13%), but lower than those for the bending case (3.73% and 0.69%). In the constant-life diagram (Fig. 7c), there is a significantly

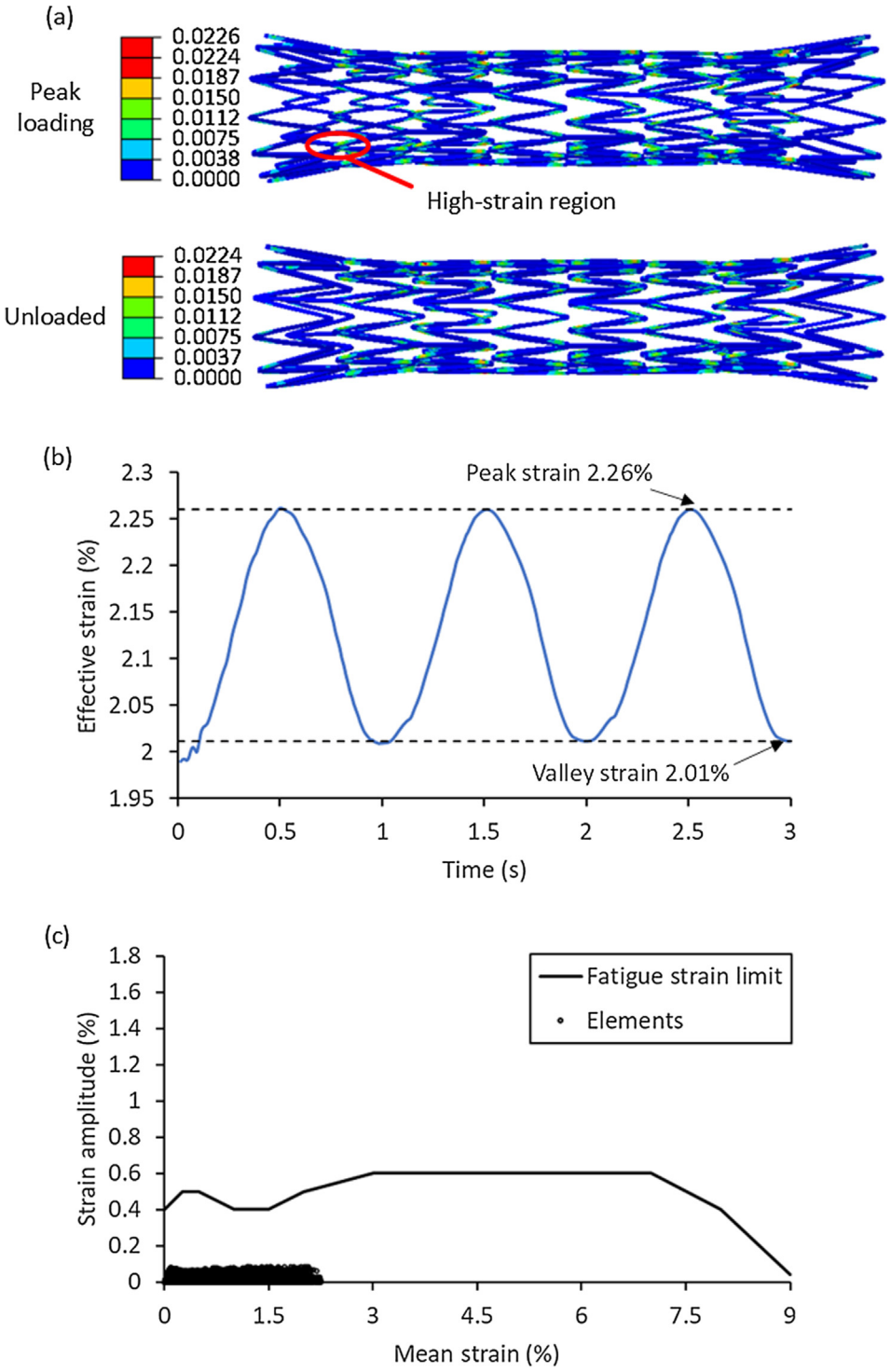


Fig. 6. Fatigue performance under torsion: (a) contour plots of effective strain in stent at peak loading and unloaded conditions; (b) evolution of effective strain in high-strain region in (a) where time refers to the period of cyclic loading; (c) constant-life diagram.

increased risk of fatigue failure when compared to the torsion case, but not as risky as the bending case.

3.5. Fatigue performance under combined loadings

Fig. 8a shows the effective strain distribution of the stent at the peak loading and unloaded conditions under combined loadings of bending, torsion and axial compression. Similar to the other cases, the maximum strain in the stent at the peak load was higher than that at the unloaded condition (3.13% *vs.* 2.75%). Its evolution of effective strain is plotted in Fig. 8b, which tended to stabilize after 1 cycle. It showed the highest stabilized peak strain (4.58%) and strain amplitude (0.92%) among all the cases. In the constant-life diagram (Fig. 8c), many elements are in the dangerous zone above the fatigue strain limit line, indicating the highest risk of fatigue failure among all loading scenarios.

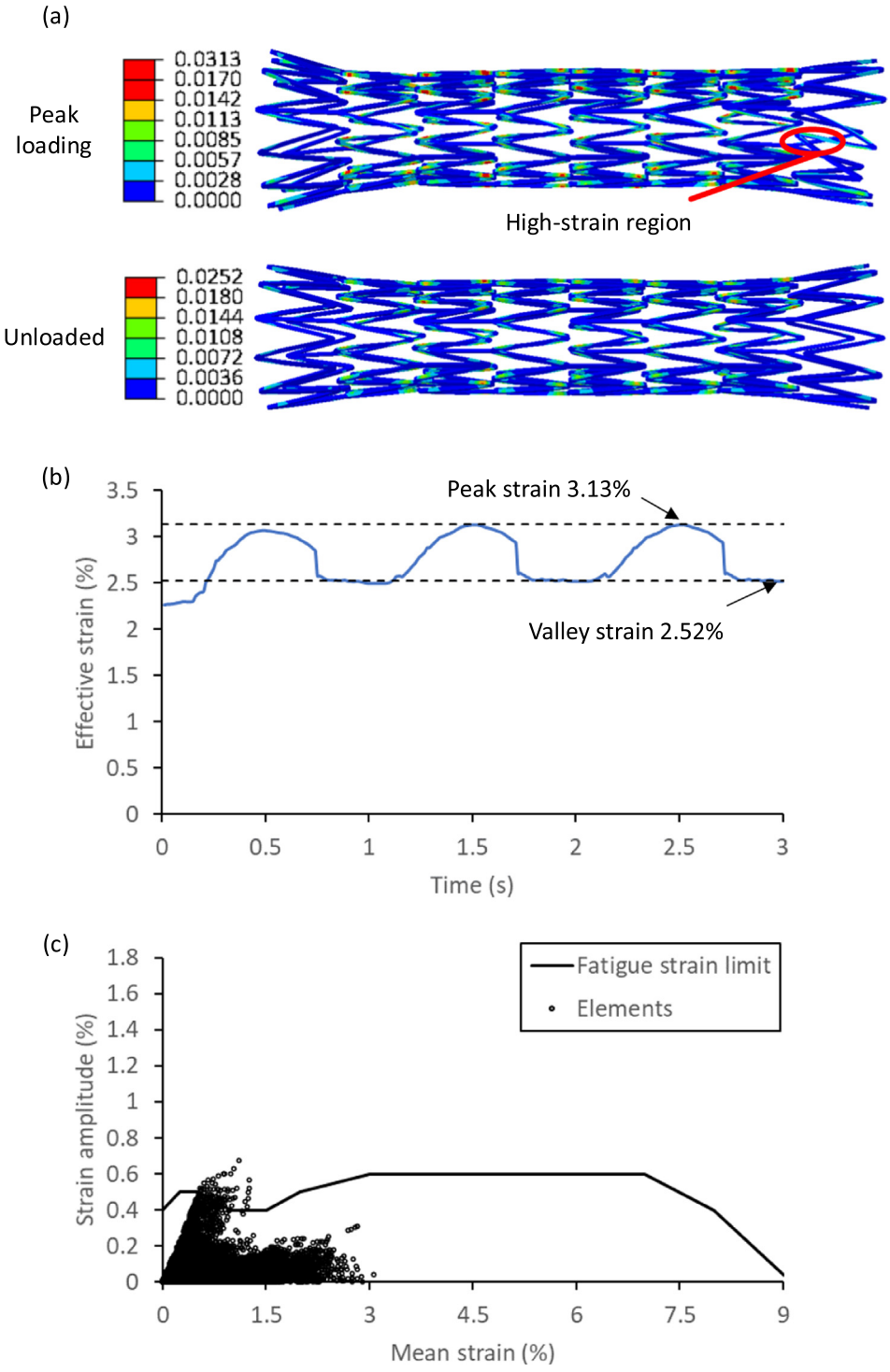


Fig. 7. Fatigue performance under axial compression: (a) contour plots of effective strain in stent at peak loading and unloaded conditions; (b) evolution of effective strain in high-strain region in (a) where time refers to the period of cyclic loading; (c) constant-life diagram.

4. Discussion

This study is the first attempt to investigate the fatigue resistance of nitinol stents subjected to walk-induced femoropopliteal artery motion. Particularly, the bending, torsion and axial compression applied to the implanted stent were taken from measurements of human femoropopliteal artery motion using the intra-arterial markers (Desyatova et al., 2017; Poulson et al., 2018; MacTaggart et al., 2019). Similar computational studies were reported in the literature, but limited to two-dimensional data, which gave inadequate information of bending and axial compression (Early and Kelly, 2011; Harvey, 2011; Petrini et al., 2012; Dordoni et al., 2014; Lei et al., 2019). Some studies even applied unrealistic loading frequency, such as 50 Hz in Lei et al. (2019), in simulations; while the realistic one was measured to be 1 Hz (Ji and Pachi, 2005). In dynamic analysis, this may result in higher levels of mean strain or strain amplitude in the stent due to inertia, leading to overestimated risk of fatigue failure. Also, the simulated

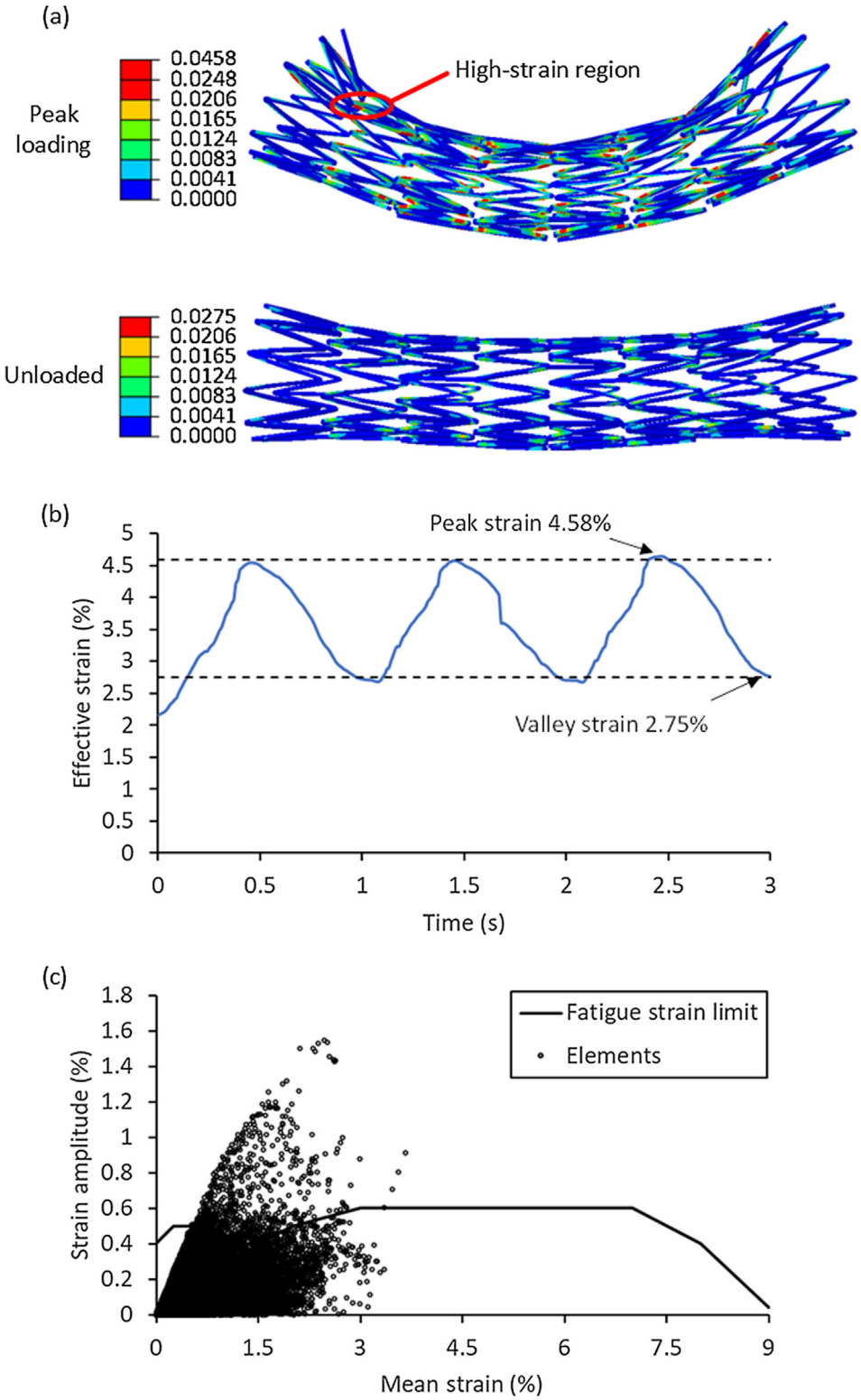


Fig. 8. Fatigue performance under combined loadings: (a) contour plots of effective strain in stent at peak loading and unloaded conditions; (b) evolution of effective strain in high-strain region in (a) where time refers to the period of cyclic loading; (c) constant-life diagram.

strain in the stent normally took some cycles to stabilize in this study, as also reported in Dordoni et al. (2014). However, some studies only simulated one cycle (Lei et al., 2019) or just a loading phase (Early and Kelly, 2011; Harvey, 2011), which might result in erroneous assessment of stent's fatigue failure.

Walking predisposes stent fracture in patients with nitinol stents implanted in the femoropopliteal arteries (Iida et al., 2006), especially if implanted at or near the flexion points in the femoropopliteal arteries (Babalik et al., 2003). Since stent fracture is associated with in-stent restenosis or lumen reocclusion

(Scheinert et al., 2005), it is important to understand the fatigue behaviour of nitinol stents implanted in femoropopliteal artery under physiological and biomechanical loading conditions. Our results showed that the pulsatile blood pressure did not contribute much to stent's fatigue failure (Fig. 4c), agreeing with the experimental results in Pelton et al. (2008). Thus, it was not considered in the combined loading case. Similar to the work of Lei et al. (2019), the combined loading imposed the highest risk to stent's fatigue failure. The main contribution was bending, followed by axial compression and torsion, in contrast to the works of Early and Kelly (2011) and Dordoni et al. (2014). However, no study investigated the effect of torsion fatigue on stent failure. Our simulations predicted a lower risk of fatigue failure of the nitinol stent when subjected to torsion when compared to axial compression and bending.

It is well known that the bending, torsion and axial motions are at a rate of 10^6 cycles per year (Silva et al., 2002). In this study, the fatigue limit was assessed against a life of 10^7 cycles obtained from fatigue testing of diamond-shape nitinol specimens (Pelton, 2011), and, therefore, the predicted life in service is at least ten years. The manufacturing process of these diamond-shape specimens followed the actual process of commercial stents, representing the material properties and relative geometry of the actual product as close as possible, and tested at a temperature of 37 °C. However, it should be noted that different medical device companies use different manufacturing and thermo-mechanical processes which can induce different fatigue properties in nitinol. Thus, for proper evaluation of the fatigue behaviour of the Zilver stent studied in this paper, ad hoc fatigue testing should be performed. In particular, specimens of similar size to the Zilver stent struts, subjected to the same manufacturing route, should be used.

This study showed the feasibility of predicting stent fatigue failure and establishing its relationship with femoropopliteal environment using the FE method. By managing the fatigue behaviour of nitinol stents, better and safer stents with innovative designs could be developed to optimise clinical outcomes. Nevertheless, there are some limitations of this study. In addition to normal walking, Desyatova et al. (2017) and Poulson et al. (2018) measured deformations of femoropopliteal arteries in sitting and gardening postures. Their results showed that these postures caused increased deformations in the artery, which may result in higher levels of mean strain and strain amplitude in the implanted nitinol stent. However, as most people usually do not change from sitting or gardening to standing postures frequently, they may not cause so high risk of stent's fatigue failure as daily walk. Additionally, different stents showed varying levels of resistances to different loadings in mechanical testing (Maleckis et al., 2017; MacTaggart et al., 2019). Hence, it may be also interesting to investigate the effect of different stents implanted in femoropopliteal arteries on their fatigue behaviours subjected to respective deformations. Obviously, in the simulations, the nitinol stent was considered ideal without any defects, but it is widely recognized that some cracks or defects exist in materials. For instance, laser-cutting used to fabricate stents invariably leaves a distribution of small cracks (5 to 20 μm) on the surface (McKelvey and Ritchie, 1999). As the fatigue-limit analyses are unable to assess the fracture risks of stents with pre-existing defects/cracks, other approaches such as fracture mechanics with a damage-tolerance concept is required in the future work.

Also, it was found that, due to high axial stiffness of nitinol stents, the stented femoropopliteal artery was compressed in knee flexion less than the unstented one (MacTaggart et al., 2019). The increased axial stiffness may reduce the ability of arteries to accommodate foreshortening, resulting in kinks of the transition zone between the stented and unstented regions. This may affect the fatigue behaviour of nitinol stents. In addition, the plaque model was idealized as a single, uniform and symmetric layer; while, in reality, the plaque normally has a complex morphology and often not concentric with varied mechanical properties. Therefore, the contact between the plaque/artery and stent may be very different from the current model, which may increase local strain concentration and shorten the fatigue life of the deployed nitinol stent. Hence, to gain a better understanding of the effect of arterial kinks and to apply the current approach to clinical conditions, patient-specific models are recommended in future studies, based on high-resolution medical imaging of actual diseased artery (He et al., 2020c).

Declaration of Competing Interest

The authors declare that they have no known competing financial interests or personal relationships that could have appeared to influence the work reported in this paper.

Acknowledgements

We acknowledge the support from the EPSRC UK (Grant number: EP/R001650/1; Title: Smart peripheral stents for the lower extremity - design, manufacturing and evaluation). Research data for this paper are available upon request to the projects' principal investigator Professor Liguo Zhao at Loughborough University, UK (email: L.Zhao@Lboro.ac.uk).

Appendix A. Supplementary material

Supplementary data to this article can be found online at https://doi.org/10.1016/j.jbiomech.2021.110295.

References

Allegretti, D., Berti, F., Migliavacca, F., Pennati, G., Petrini, L., 2018. Fatigue assessment of nickel–titanium peripheral stents: Comparison of multi-axial fatigue models. Shape Memory Superelasticity 4, 186–196. https://doi.org/10.1007/s40830-018-0150-7.

Ansari, F., Pack, L.K., Brooks, S.S., Morrison, T.M., 2013. Design considerations for studies of the biomechanical environment of the femoropopliteal arteries. J. Vasc. Surg. 58 (3), 804–813. https://doi.org/10.1016/j.jvs.2013.03.052.

Aoi, S., Ohashi, T., Bamba, R., Fujiki, S., Tamura, D., Funato, T., Senda, K., Ivanenko, Y., Tsuchiya, K., 2019. Neuromusculoskeletal model that walks and runs across a speed range with a few motor control parameter changes based on the muscle synergy hypothesis. Sci. Rep. 9, 369. https://doi.org/10.1038/s41598-018-37460-3.

Azaouzi, M., Lebaal, N., Makradi, A., Belouettar, S., 2013. Optimization based simulation of self-expanding Nitinol stent. Mater. Des. 50, 917–928. https://doi.org/10.1016/j.matdes.2013.03.012.

Babalik, E., Gülbaran, M., Gürmen, T., Öztürk, S., 2003. Fracture of popliteal artery stents. Circ. J. 67, 643–645. https://doi.org/10.1253/circj.67.643.

Cheng, C.P., Choi, G., Herfkens, R.J., Taylor, C.A., 2010. The effect of aging on deformations of the superficial femoral artery resulting from hip and knee flexion: Potential clinical implications. J. Vasc. Interv. Radiol. 21 (2), 195–202. https://doi.org/10.1016/j.jvir.2009.08.027.

Cheng, C.P., Wilson, N.M., Hallett, R.L., Herfkens, R.J., Taylor, C.A., 2006. In vivo MR angiographic quantification of axial and twisting deformations of the superficial femoral artery resulting from maximum hip and knee flexion. J. Vasc. Interv. Radiol. 17 (6), 979–987. https://doi.org/10.1097/01.RVI.0000220367.62137.e8.

Desyatova, A., Poulson, W., Deegan, P., Lomneth, C., Seas, A., Maleckis, K., MacTaggart, J., Kamenskiy, A., 2017. Limb flexion-induced twist and associated intramural stresses in the human femoropopliteal artery. J. R. Soc. Interface 14 (128), 20170025. https://doi.org/10.1098/rsif.2017.0025.

Dordoni, E., Meoli, A., Wu, W., Dubini, G., Migliavacca, F., Pennati, G., Petrini, L., 2014. Fatigue behaviour of nitinol peripheral stents: The role of plaque shape studied with computational structural analyses. Med. Eng. Phys. 36 (7), 842–849. https://doi.org/10.1016/j.medengphy.2014.03.006.

Dordoni, E., Petrini, L., Wu, W., Migliavacca, F., Dubini, G., Pennati, G., 2015. Computational modeling to predict fatigue behavior of NiTi stents: What do we need?. J. Funct. Biomater. 6 (2), 299–317. https://doi.org/10.3390/jfb6020299.

Duda, S.H., Bosiers, M., Lammer, J., Scheinert, D., Zeller, T., Oliva, V., Tielbeek, A., Anderson, J., Wiesinger, B., Tepe, G., Lansky, A., Jaff, M.R., Mudde, C., Tielemans, H., Beregi, J.P., 2006. Drug-eluting and bare nitinol stents for the treatment of atherosclerotic lesions in the superficial femoral artery: Long-term results from

the SIROCCO trial. J. Endovascular Therapy 13 (6), 701–710. https://doi.org/10.1583/05-1704.1.
Early, M., Kelly, D.J., 2011. The consequences of the mechanical environment of peripheral arteries for nitinol stenting. Med. Biol. Eng. Compu. 49, 1279–1288. https://doi.org/10.1007/s11517-011-0815-2.
Elens, M., Verhelst, R., Mastrobuoni, S., Bosiers, M.J., Possoz, J., Lacroix, V., Astarci, P., 2019. Balloon angioplasty versus bailout stenting for isolated chronic total occlusions in the popliteal artery. Vascular Endovascular Surgery 53 (2), 126–131. https://doi.org/10.1177/1538574418814060.
Fargion, A., Masciello, F., Pratesi, G., Giacomelli, E., Dorigo, W., Pratesi, C., 2017. Endovascular Treatment with Primary Stenting of Acutely Thrombosed Popliteal Artery Aneurysms. Ann. Vasc. Surg. 44, 421.e5–421.e8. https://doi.org/10.1016/j.avsg.2017.04.027.
Fereidoonnezhad, B., Naghdabadi, R., Holzapfel, G.A., 2016. Stress softening and permanent deformation in human aortas: Continuum and computational modeling with application to arterial clamping. J. Mech. Behav. Biomed. Mater. 61, 600–616. https://doi.org/10.1016/j.jmbbm.2016.03.026.
Fusaro, M., Cassese, S., Ndrepepa, G., King, L.A., Tada, T., Ott, I., Kastrati, A., 2013. Paclitaxel-coated balloon or primary bare nitinol stent for revascularization of femoropopliteal artery: A meta-analysis of randomized trials versus uncoated balloon and an adjusted indirect comparison. Int. J. Cardiol. 168 (4), 4002–4009. https://doi.org/10.1016/j.ijcard.2013.06.081.
Goodfellow, 2018. Polyethylene terephthalate (Polyester, PET, PETP) Material Information. http://www.goodfellow.com/E/Polyethylene-terephthalate.html.
Harvey, S.M., 2011. Nitinol stent fatigue in a peripheral human artery subjected to pulsatile and articulation Loading. J. Mater. Eng. Perform. 20, 697–705. https://doi.org/10.1007/s11665-011-9881-8.
He, R., Zhao, L.G., Silberschmidt, V.V., Liu, Y., 2020a. Mechanistic evaluation of long-term in-stent restenosis based on models of tissue damage and growth. Biomech. Model. Mechanobiol. 1–22. https://doi.org/10.1007/s10237-019-01279-2.
He, R., Zhao, L.G., Silberschmidt, V.V., Liu, Y., Vogt, F., 2020b. Finite element evaluation of artery damage in deployment of polymeric stent with pre- and post-dilation. Biomech. Model. Mechanobiol. 19 (1), 47–60. https://doi.org/10.1007/s10237-019-01194-6.
He, R., Zhao, L.G., Silberschmidt, V.V., Liu, Y., Vogt, F., 2020c. Patient-specific modelling of stent overlap: Lumen gain, tissue damage and in-stent restenosis. J. Mech. Behav. Biomed. Mater. 109,. https://doi.org/10.1016/j.jmbbm.2020.103836 103836.
Henry, M., Amor, M., Ethevenot, G., Henry, I., Amicabile, C., Beron, R., Mentre, B., Allaoui, M., Touchot, N., 1995. Palmaz stent placement in iliac and femoropopliteal arteries: Primary and secondary patency in 310 patients with 2–4-year follow-up. Radiology 197 (1), 167–174. https://doi.org/10.1148/radiology.197.1.7568818.
Heuser, R.R., Henry, M., 2008. Textbook of Peripheral Vascular Interventions. Taylor & Francis US. https://doi.org/10.3109/9781439801970.
Iida, O., Nanto, S., Uematsu, M., Morozumi, T., Kotani Ichi, J., Awata, M., Onishi, T., Ito, N., Sera, F., Minamiguchi, H., Akahori, H., Nagata, S., 2006. Effect of exercise on frequency of stent fracture in the superficial femoral artery. Am. J. Cardiol. 98 (2), 272–274. https://doi.org/10.1016/j.amjcard.2006.01.091.
Jeans, W.D., Armstrong, S., Cole, S.E.A., Horrocks, M., Baird, R.N., 1990. Fate of patients undergoing transluminal angioplasty for lower-limb ischemia. Radiology 177 (2), 559–564. https://doi.org/10.1148/radiology.177.2.2145608.
Ji, T., Pachi, A., 2005. Frequency and velocity of people walking. Struct. Eng. 84 (3), 36–40.
Kim, H.T., Cho, J.H., Lee, J.H., Kim, U., 2020. Early Supera stent fracture in the femoropopliteal artery. Cardiovascular J. Africa 31, 1–3. https://doi.org/10.5830/CVJA-2020-004.
Klein, A.J., Chen, S.J., Messenger, J.C., Hansgen, A.R., Plomondon, M.E., Carroll, J.D., Casserly, I.P., 2009. Quantitative assessment of the conformational change in the femoropopliteal artery with leg movement. Catheterization Cardiovascular Intervent. 74 (5), 787–798. https://doi.org/10.1002/ccd.22124.
Laird, J.R., Katzen, B.T., Scheinert, D., Lammer, J., Carpenter, J., Buchbinder, M., Dave, R., Ansel, G., Lansky, A., Cristea, E., Collins, T.J., Goldstein, J., Jaff, M.R., 2010. Nitinol stent implantation versus balloon angioplasty for lesions in the superficial femoral artery and proximal popliteal artery: Twelve-month results from the RESILIENT randomized trial. Circulation: Cardiovascular Intervent. 3 (3), 267–276. https://doi.org/10.1161/CIRCINTERVENTIONS.109.903468.
Lei, L., Qi, X., Li, S., Yang, Y., Hu, Y., Li, B., Zhao, S., Zhang, Y., 2019. Finite element analysis for fatigue behaviour of a self-expanding Nitinol peripheral stent under physiological biomechanical conditions. Comput. Biol. Med. 104, 205–214. https://doi.org/10.1016/j.compbiomed.2018.11.019.
MacTaggart, J.N., Phillips, N.Y., Lomneth, C.S., Pipinos, I.I., Bowen, R., Timothy Baxter, B., Johanning, J., Matthew Longo, G., Desyatova, A.S., Moulton, M.J., Dzenis, Y.A., Kamenskiy, A.V., 2014. Three-dimensional bending, torsion and axial compression of the femoropopliteal artery during limb flexion. J. Biomech. 47 (10), 2249–2256. https://doi.org/10.1016/j.jbiomech.2014.04.053.
MacTaggart, J., Poulson, W., Seas, A., Deegan, P., Lomneth, C., Desyatova, A., Maleckis, K., Kamenskiy, A., 2019. Stent design affects femoropopliteal artery deformation. Ann. Surg. 270 (1), 180–187. https://doi.org/10.1097/SLA.0000000000002747.
Maleckis, K., Deegan, P., Poulson, W., Sievers, C., Desyatova, A., MacTaggart, J., Kamenskiy, A., 2017. Comparison of femoropopliteal artery stents under axial and radial compression, axial tension, bending, and torsion deformations. J. Mech. Behav. Biomed. Mater. 75, 160–168. https://doi.org/10.1016/j.jmbbm.2017.07.017.
McKelvey, A.L., Ritchie, R.O., 1999. Fatigue-crack propagation in Nitinol, ashape-memory and superelastic endovascular stent material. J. Biomed. Mater. Res. 47 (3), 301–308. https://doi.org/10.1002/(SICI)1097-4636(19991205)47:3<301::AID-JBM3>3.0.CO;2-H.
Meoli, A., Dordoni, E., Petrini, L., Migliavacca, F., Dubini, G., Pennati, G., 2013. Computational modelling of in vitro set-ups for peripheral self-expanding nitinol stents: The importance of stent-wall interaction in the assessment of the fatigue resistance. Cardiovascular Eng. Technol. 4, 474–484. https://doi.org/10.1007/s13239-013-0164-4.
Meoli, A., Dordoni, E., Petrini, L., Migliavacca, F., Dubini, G., Pennati, G., 2014. Computational study of axial fatigue for peripheral nitinol stents. J. Mater. Eng. Perform. 23, 2606–2613. https://doi.org/10.1007/s11665-014-0965-0.
Mewissen, M.W., 2004. Self-expanding nitinol stents in the femoropopliteal segment: Technique and mid-term results. Tech. Vascular Intervent. Radiol. 7 (1), 2–5. https://doi.org/10.1053/j.tvir.2004.01.007.
Nolan, D.R., Gower, A.L., Destrade, M., Ogden, R.W., McGarry, J.P., 2014. A robust anisotropic hyperelastic formulation for the modelling of soft tissue. J. Mech. Behav. Biomed. Mater. 39, 48–60. https://doi.org/10.1016/j.jmbbm.2014.06.016.
Ogden, R.W., 1972. Large deformation isotropic elasticity—on the correlation of theory and experiment for incompressible rubberlike solids. Rubber Chem. Technol. 46 (1567), 565–584. https://doi.org/10.5254/1.3542910.
Ogden, R.W., Roxburgh, D.G., 1999. A pseudo-elastic model for the Mullins effect in filled rubber. Proc. Roy. Soc. A: Math., Phys. Eng. Sci. 455 (1988), 2861–2877. https://doi.org/10.1098/rspa.1999.0431.
Pelton, A.R., 2011. Nitinol fatigue: A review of microstructures and mechanisms. J. Mater. Eng. Perform. 20 (4–5), 613–617. https://doi.org/10.1007/s11665-011-9864-9.
Pelton, A.R., Schroeder, V., Mitchell, M.R., Gong, X.Y., Barney, M., Robertson, S.W., 2008. Fatigue and durability of Nitinol stents. J. Mech. Behav. Biomed. Mater. 1 (2), 153–164. https://doi.org/10.1016/j.jmbbm.2007.08.001.
Petrini, L., Trotta, A., Dordoni, E., Migliavacca, F., Dubini, G., Lawford, P.V., Gosai, J.N., Ryan, D.M., Testi, D., Pennati, G., 2016. A computational approach for the prediction of fatigue behaviour in peripheral stents: Application to a clinical case. Ann. Biomed. Eng. 44, 536–547. https://doi.org/10.1007/s10439-015-1472-7.
Petrini, L., Wu, W., Dordoni, E., Meoli, A., Migliavacca, F., Pennati, G., 2012. Fatigue behavior characterization of nitinol for peripheral stents. Funct. Mater. Lett. 5 (1), 1250012. https://doi.org/10.1142/S1793604712500129.
Poulson, W., Kamenskiy, A., Seas, A., Deegan, P., Lomneth, C., MacTaggart, J., 2018. Limb flexion-induced axial compression and bending in human femoropopliteal artery segments. J. Vasc. Surg. 67 (2), 607–613. https://doi.org/10.1016/j.jvs.2017.01.071.
Qiu, T., He, R., Abunassar, C., Hossainy, S., Zhao, L.G., 2018. Effect of two-year degradation on mechanical interaction between a bioresorbable scaffold and blood vessel. J. Mech. Behav. Biomed. Mater. 78, 254–265. https://doi.org/10.1016/j.jmbbm.2017.11.031.
Reis, J. M. C. dos, Kudo, F. A., Carmo Bastos, M. do., 2019. Fracture of a popliteal nitinol stent and pseudoaneurysm: a case report and review of the literature. J. Surgical Case Reports, 11, 1–3. https://doi.org/10.1093/jscr/rjz312.
San Norberto, E.M., Fuente, R., Flota, C.M., Taylor, J.H., Vaquero, C., 2017. Impact of Implantation Defects on Intermediate Outcome of Supera Stent for Popliteal Artery Stenosis. Ann. Vasc. Surg. 41, 186–195. https://doi.org/10.1016/j.avsg.2016.09.021.
Saxon, R.R., Coffman, J.M., Gooding, J.M., Natuzzi, E., Ponec, D.J., 2003. Long-term results of ePTFE stent-graft versus angioplasty in the femoropopliteal artery: Single center experience from a prospective, randomized trial. J. Vasc. Interv. Radiol. 14 (3), 303–311. https://doi.org/10.1097/01.RVI.0000058425.01661.d0.
Scheinert, D., Scheinert, S., Sax, J., Piorkowski, C., Bräunlich, S., Ulrich, M., Biamino, G., Schmidt, A., 2005. Prevalence and clinical impact of stent fractures after femoropopliteal stenting. J. Am. Coll. Cardiol. 45 (2), 312–315. https://doi.org/10.1016/j.jacc.2004.11.026.
Schillinger, M., Sabeti, S., Loewe, C., Dick, P., Amighi, J., Mlekusch, W., Schlager, O., Cejna, M., Lammer, J., Minar, E., 2006. Balloon angioplasty versus implantation of nitinol stents in the superficial femoral artery. N. Engl. J. Med. 354 (18), 1879–1888. https://doi.org/10.1056/NEJMoa051303.
Sibé, M., Kaladji, A., Boirat, C., Cardon, A., Chaufour, X., Bossavy, J.P., Saint-Lebes, B., 2017. French multicenter experience with the GORE TIGRIS Vascular Stent in superficial femoral and popliteal arteries. J. Vasc. Surg. 65 (5), 1329–1335. https://doi.org/10.1016/j.jvs.2016.11.056.
Silva, M., Shepherd, E.F., Jackson, W.O., Dorey, F.J., Schmalzried, T.P., 2002. Average patient walking activity approaches 2 million cycles per year: Pedometers under-record walking activity. J. Arthroplasty 17 (6), 693–697. https://doi.org/10.1054/arth.2002.32699.
Vogel, T.R., Shindelman, L.E., Nackman, G.B., Graham, A.M., Silva, M.B., Rivers, S.P., Ricotta, J.J., O'Donnell, S.D., Dosluoglu, H., Kent, K.C., 2003. Efficacious use of nitinol stents in the femoral and popliteal arteries. J. Vasc. Surg. 38 (6), 1178–1183. https://doi.org/10.1016/j.jvs.2003.09.011.
Wong, M., Edelstein, J., Wollman, J., Bond, M.G., 1993. Ultrasonic-pathological comparison of the human arterial wall: Verification of intima-media thickness. Arterioscler. Thromb. Vasc. Biol. 13 (4), 482–486. https://doi.org/10.1161/01.ATV.13.4.482.